Supporting Information

Super-efficient Fire Safety Poly(lactide) Enabled by Unique Radical Trapping

Dan Xiao [a]*, Song Chen [a], Fang-Juan Wu [a], Zhi-Yu Xiao [b], Zi-Bo Wang [a], and Hui Fang [a]

[a] *Key Laboratory of Polymer Materials and Products of Universities in Fujian, Department of Materials Science and Engineering, Fujian University of Technology, Fuzhou, Fujian, 350108, China*

[b] *School of Materials Science and Engineering, Guilin University of Electronic Technology, Guilin, 541004, China*

Corresponding author:

*Email: 19872102@fjut.edu.cn, Tel:+86 0591 6233152 (D. Xiao)

Experimental procedures

Materials

Synthesis of F-FR

Fabrication of PLA/F-FR composites

Structural characterization

Thermal stability analysis

Fire safety performance

Condensed phase analysis

Pyrolysis analysis

Computational simulation analysis

Crystallization behavior

Mechanical properties analysis

Transparency analysis

EXPERIMENTAL PROCEDURES

Materials

PLA (3052D) was manufactured by Nature-Works (USA); phenylphosphoryl dichloride (urity>98%) was obtained from Macklin Reagent Co., Ltd. (China); tetrahydrofurfurylamine and furfurylamine (urity>98%) were purchased from Aladdin Chemical Reagent Co., Ltd. (China); dichloromethane (urity>98%) and triethylamine (urity>98%) was purchased from Sinopharm Chemical Reagent (China).

Synthesis of F-FR

Tetrahydrofurfurylamine (22 mmol) and triethylamine (22 mmol) were dissolved in the dichloromethane under N_2 atmosphere. Then phenylphosphoryl dichloride (10 mmol) for 2 hours was added under 0 - 5 ˚C environment. After that, the temperature warmed up the room temperature for 20 hours. The mixture was separated by a Buchner funnel. Afterwards, the filtrate was purified multiple times using water. Finally, the light yellow liquid F-FR was steamed and obtained in vacuum at 60 ˚C. The synthetic route of F-FR was shown in Figure 1S.

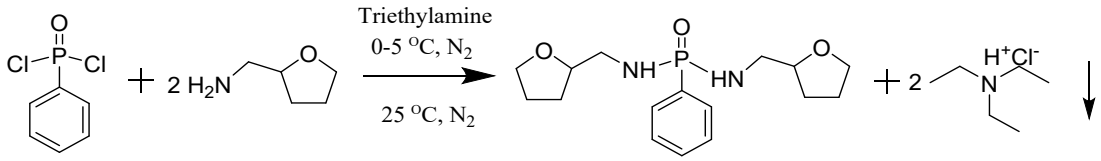

Figure 1S. Synthesis route of F-FR

Fabrication of PLA/F-FR composites

Dried PLA with different loading F-FR were plasticized by torque rheometer Polylab OS mixer with 70 rpm/min at 175 ˚C for 5 min. After that, the specimens with desired dimensions 185 ˚C were pressed by a CREE-6014A-30 hot presses. Finally, the specimens for the tensile testing at 175 ºC were prepared by injection molding (Donghua Machinery, China).

Structure characterization

^{1}H NMR measurement was carried out using a DRX Bruker 400 MHz instrument using $CDCl_3$ as the solvent. FT-IR result was conducted using a Nicolet Thermo 6700 instrument. MS testing was investigated by an Agilent 5977 B instrument (America).

Fire safety measurements

The UL-94 Vertical burning (size: 13 mm × 130 mm × 3 mm) measurement was conducted on a CZF-2 Jiangning measurement in accordance with ASTM D 3801 standard. LOI (size: 6.5 mm × 120 mm × 3 mm) measurement was investigated by a JF-3 Jiangning measurement in accordance with ASTM D2863 standard. Cone-calorimeter (100 mm × 3 mm × 100 mm) measurement was investigated by a FTT measurement (35 kW/m^2, Britain) in accordance with ISO 5660-1 standard.

Thermal behavior measurements

TGA testing was investigated by a DSC 200F3 Netzsch measurement in nitrogen and air atmosphere at 10 $K \cdot min^{-1}$ from 50-700 ˚C.

Tensile measurements

Tensile (TS, size: 165 ×13 ×3.2 mm^3) measurement was conducted on an Instron 2382 instrument at the stretch rate of 10 $mm \cdot min^{-1}$.

Dynamic mechanical analysis measurements

DMA (size: 120 × 1 × 4 mm^3) measurement was conducted on a Q 800 apparatus TA instrument (three-point bending model).

Crystallization behavior measurements

DSC testing was investigated by a DSC 200F3 Netzsch measurement. For non-

isothermal crystallization behavior, the specimens (5.0-10.0 mg) were firstly heated to eliminate heat history. After that, the composites were secondly heated up to 200 ˚C. For isothermal crystallization testing, the specimens (5-10 mg) was firstly treated with the same procedure at 80 $K \cdot min^{-1}$ to eliminate thermal history on a DSC 200F3 Netzsch under N_2, and then cooled to a predetermined temperature (100°C, 105°C, 110°C, 115°C), and record the curve of isothermal crystallization. Polarizing optical microscope (POM) measurement was conducted on a DM 2700P LEICA instrument.

Fire safety mechanism analysis

SEM testing was investigated by a JEOL JSM-6700F measurement. Raman testing was carried out using a Thermo Fisher DxRxi instrument. Py-GC-MS testing was investigated by an Agilent 5977 B connected with Agilent 8790 B under He atmosphere. TG-FTIR measurement was conducted on a Netzsch TG209F1 instrument connected with a Vertex70 Bruker instrument.

Fire safety mechanism simulation

The bonding energy of degradation and combustion behavior were conducted on a Material Studio software (version 2018). In this simulation, combustion products and compositions were analyzed from Py-GC-MS and TG-FTIR. The radical trapping mechanisms of HOMO and LUMO were simulated by $Dmol^3$ included in Material Studio software.

Captions of Tables

Table 1S. Thermal properties of F-FR, pure PLA and PLA/F-FR composites

Table 2S. The gas products of F-FR after degradation

Table 3S. The non-isothermal crystallization results (second heating) of pure PLA PLA/F-FR composites

Table 4S. Isothermal crystallization results of PLA and PLA/F-FR composites from Avrami formula

Table 5S. The tensile results of PLA and PLA/F-FR composites

Table 1S. Thermal properties of F-FR, pure PLA and PLA/F-FR composites

Samples	T_{onset}	T_{max}	R_{max}	Residue (%)

	(°C)	(°C)	(%/°C)	500 ˚C	600 ˚C
F-FR	205	313	1.1	17.1	16.2
PLA in N2	332	369	3.2	0.3	0.1
PLA/0.5% F-FR in N2	331	348	4.8	1.7	1.6
PLA/0.8% F-FR in N2	328	361	3.9	1.8	1.7
PLA/2% F-FR in N2	322	362	2.8	1.9	1.8
PLA in air	335	373	3.3	1.7	1.7
PLA/0.5% F-FR in air	335	376	3.5	2.6	1.7
PLA/0.8% F-FR in air	332	382	2.7	2.7	1.6
PLA/2% F-FR in air	327	380	2.2	2.5	1.7

Table 2S. The gas products of F-FR after degradation

Retention time (min)	M(g/mol)	Possible molecular structure

1.62	51.06	
1.65	52.07	
1.71	53.08	
1.73	54.04	
1.83	68.07	
1.85	69.08	
1.92	77.10	
1.95	78.11	
2.13	101.14	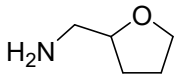
2.80	125.08	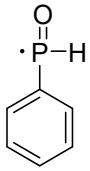
3.47	155.13	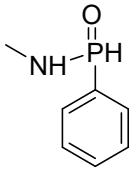
4.90	201.8	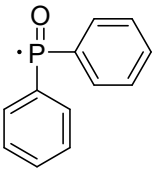
6.83	224.2	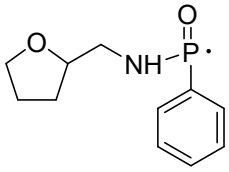

10.11	239.2	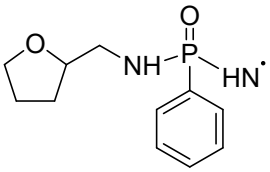
10.93	240.2	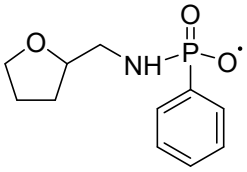
11.21	241.2	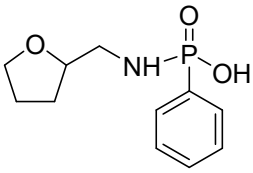
14.72	256.2	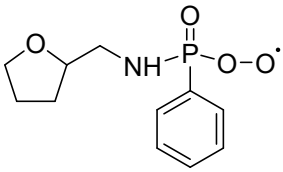
15.75	272.3	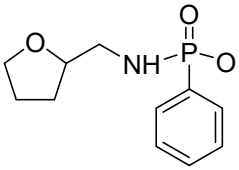
16.43	300.3	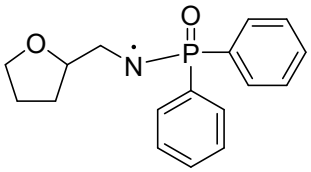
23.34	348.5	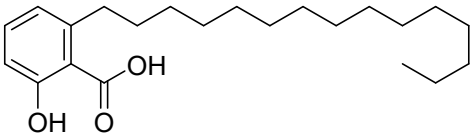
24.57	364.5	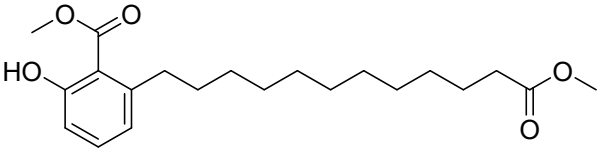

Table 3S. The non-isothermal crystallization results (second heating) of pure PLA PLA/F-FR composites

Samples	T_{cc} (˚C)	ΔH_{cc} (˚C)	T_m (˚C)	ΔH_m (J/g)	X_c (%)
PLA	107.3	30.62	170.3	36.64	6.4
PLA/0.5%F-FR	101.5	27.91	167.7	37.27	10.35
PLA/0.8% F-FR	101.4	25.65	166.2	36.02	11.17
PLA/2% F-FR	100.4	33.26	165.2	43.95	12.72

Table 4S. Isothermal crystallization results of PLA and PLA/F-FR composites from Avrami formula

Samples	T (℃)	n	lnk	k	$t_{1/2}$

PLA	100	2.32	-2.47	8.64×10^{-2}	2.48
	105	2.34	-2.45	8.60×10^{-2}	2.44
	110	2.26	-1.14	3.20×10^{-1}	1.41
	115	2.36	-2.41	9.00×10^{-2}	2.38
PLA/0.5% F-FR	100	2.29	-1.09	3.36×10^{-1}	1.37
	105	2.82	-1.27	2.81×10^{-1}	1.38
	110	2.88	-1.06	3.46×10^{-1}	1.27
	115	2.79	-0.85	4.27×10^{-1}	1.19
PLA/0.8% F-FR	100	2.79	-2.09	1.24×10^{-1}	1.85
	105	2.83	-1.23	2.92×10^{-1}	1.36
	110	2.95	-0.83	4.36×10^{-1}	1.17
	115	3.05	-1.21	3.01×10^{-1}	1.31
PLA/2% F-FR	100	2.85	-2.00	1.35×10^{-1}	1.77
	105	2.78	-1.75	1.74×10^{-1}	1.64
	110	2.73	-1.34	2.62×10^{-1}	1.43
	115	2.83	-1.71	1.81×10^{-1}	1.61

Table 5S. The tensile results of PLA and PLA/F-FR composites

Samples	Tensile strength (MPa)	Modulus (MPa)	Elongation at break (%)
PLA	65.4±1.3	2105±9	5.1±0.3
PLA/0.5%F-FR	65.2±1.8	2192±11	4.9±0.2
PLA/0.8% F-FR	61.2±2.8	2153±13	4.8±0.3
PLA/2% F-FR	56.3±4.3	2142±15	3.5±0.2

Captions of Figures

Fig. 1S. Synthesis route of F-FR

Fig. 2S. FTIR results of tetrahydrofurfurylamine, phenylphosphoryl dichloride and F-FR

Fig. 3S. ^{1}H NMR results of F-FR

Fig. 4S. MS results of F-FR

Fig. 5S. TGA results of (a) F-FR in N_2, (b) pure PLA and PLA/F-FR composites in N_2, and (c) pure PLA and PLA/F-FR composites in air, DTG results of (d) F-FR in N_2, (e) pure PLA and PLA/F-FR composites in N_2, and (a) pure PLA and PLA/F-FR composites in air

Fig. 6S. The screenshot results of (a) pure PLA, (b) PLA/0.5% F-FR, (c)PLA/0.8% F-FR and (d) PLA/2% F-FR composites in UL-94 test

Fig. 7S. Digital images results of (a) pure PLA and (b) PLA/0.8% F-FR composites; SEM of the (c) inner surface and (d) of PLA/0.8% F-FR composites after cone-calorimeter tests

Fig. 8S. Raman result of PLA/0.8% F-FR composites after cone-calorimeter tests

Fig. 9S. 3D image TG-FTIR of (a) pure PLA and (b) PLA/0.8% F-FR composites

Fig. 10S. The possible pyrolysis of PPDF and F-FR

Fig. 11S. The possible pyrolysis of PLA

Fig. 12S. The degradation or pyrolysis products were simulated by Material Studio software

Fig. 13S. Non-isothermal crystallization results of pure PLA and PLA/F-FR composites

Fig. 14S. Isothermal crystallization of ln[-ln(1-Xt)] vs. ln(t) results of pure PLA and

PLA/F-FR composites at (a)100℃, (b)105℃, (c) 110℃ and (d)115℃

Fig. 15S. POM images of pure PLA and PLA/F-FR composites at 115 ˚C for 0, 5 and 10 min

Fig. 16S The tensile results of PLA and PLA/F-FR composites

Fig. 17S The DMA results of PLA and PLA/F-FR composites

Fig. 18S. The transparency results of (a) pure PLA, (b) PLA/0.5%F-FR, (c) PLA/0.8%F-FR and (d)PLA/2%F-FR composites

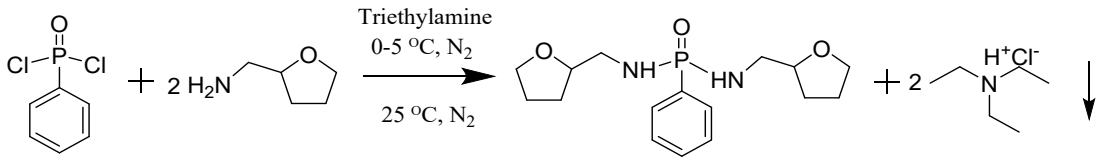

Fig. 1S. Synthesis route of F-FR

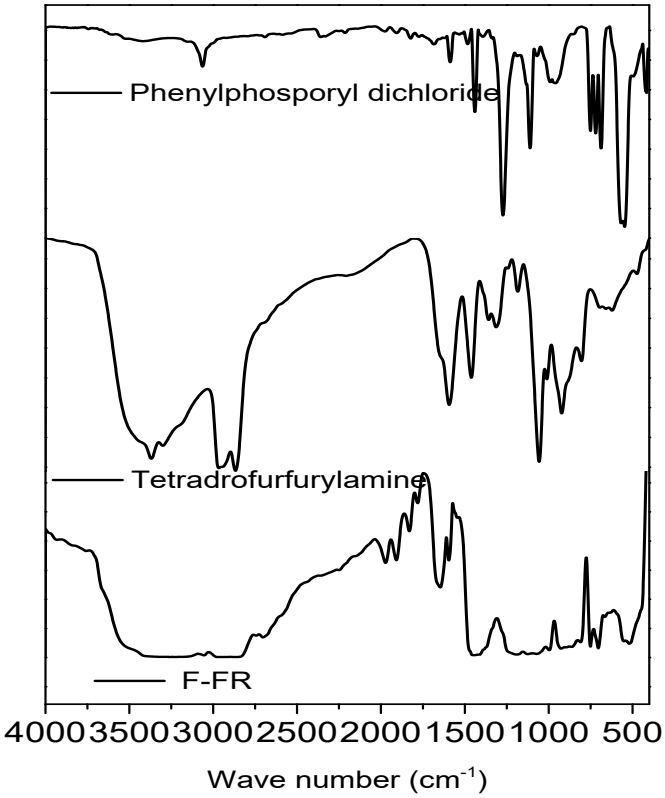

Fig. 2S. FTIR results of tetrahydrofurfurylamine, phenylphosphoryl dichloride and F-FR

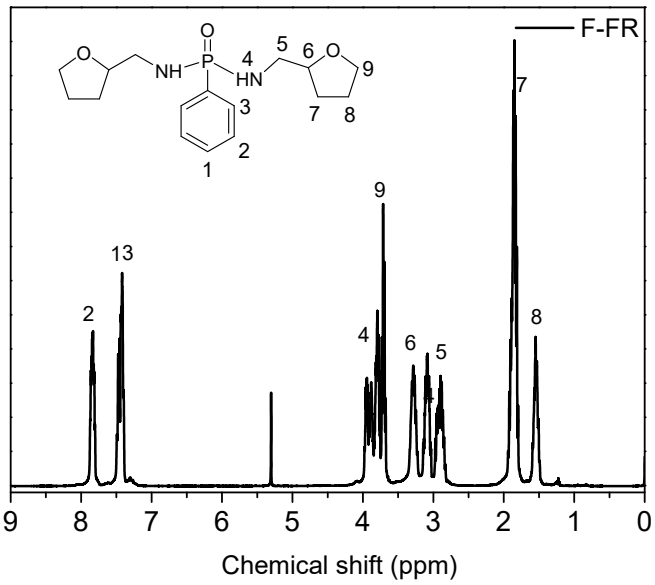

Fig. 3S. ^{1}H NMR results of F-FR

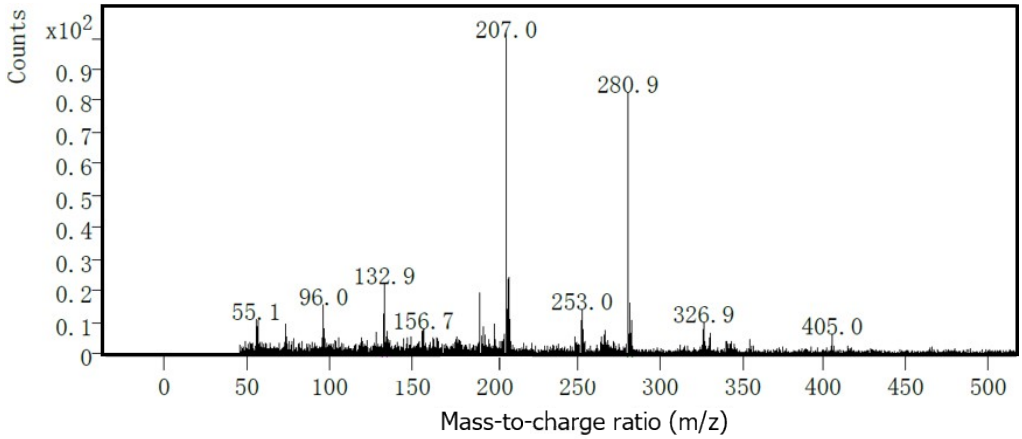

Fig. 4S. MS results of F-FR

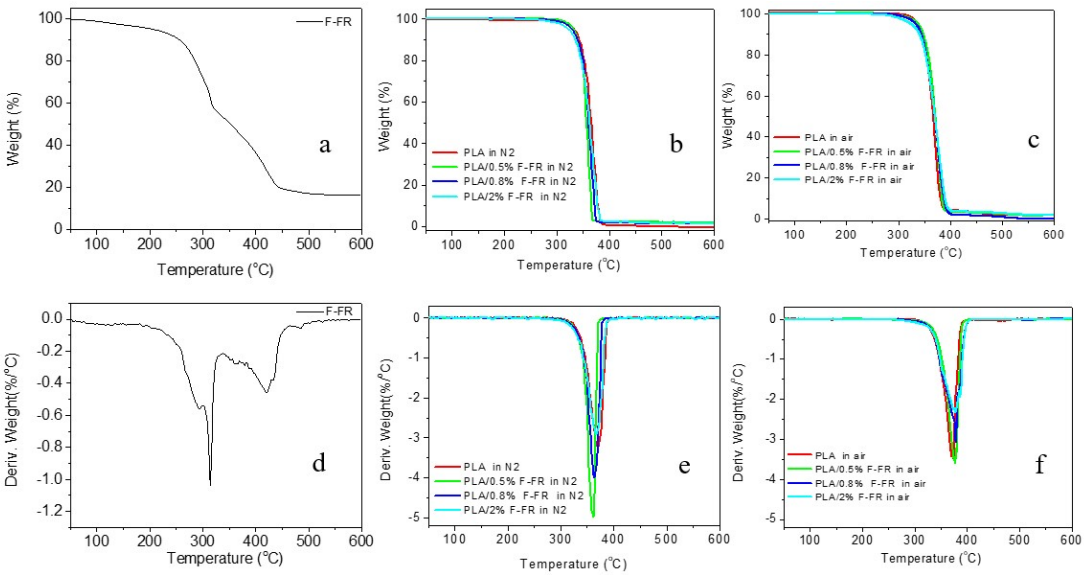

Fig. 5S. TGA results of (a) F-FR in N_2, (b) pure PLA and PLA/F-FR composites in N_2, and (c) pure PLA and PLA/F-FR composites in air, DTG results of (d) F-FR in N_2, (e) pure PLA and PLA/F-FR composites in N_2, and (f) pure PLA and PLA/F-FR composites in air

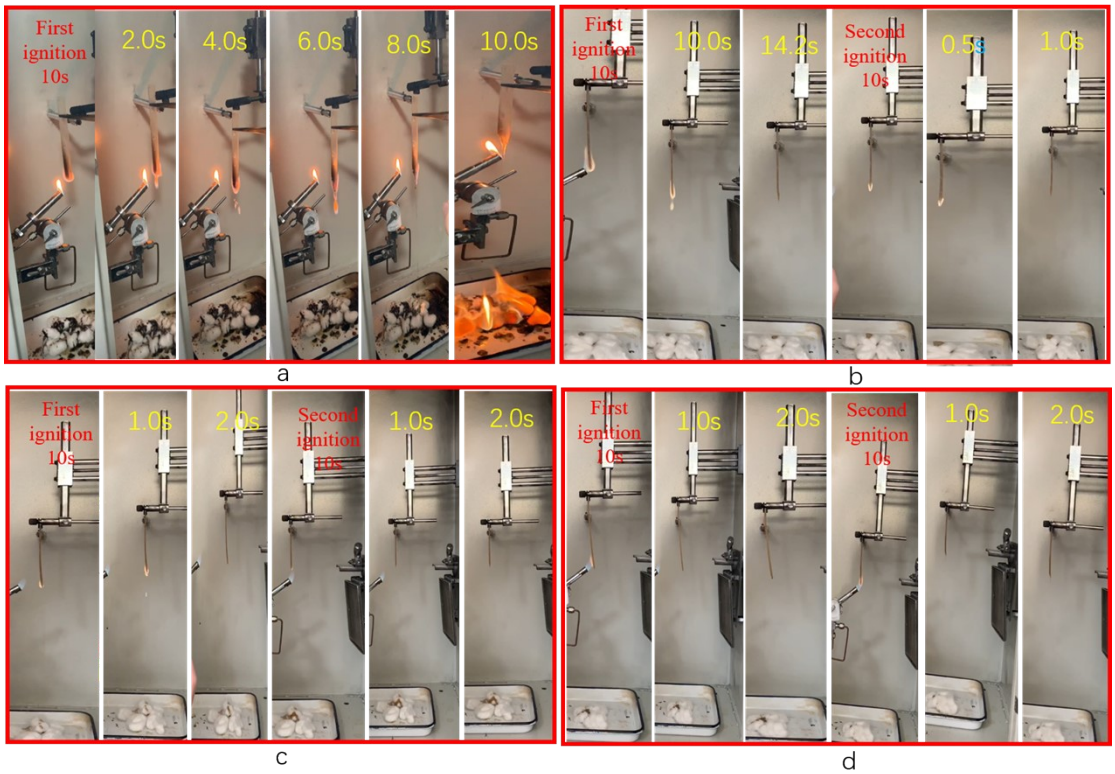

Fig. 6S. The screenshot results of (a) pure PLA, (b) PLA/0.5% F-FR, (c)PLA/0.8% F-FR and (d) PLA/2% F-FR composites in UL-94 test

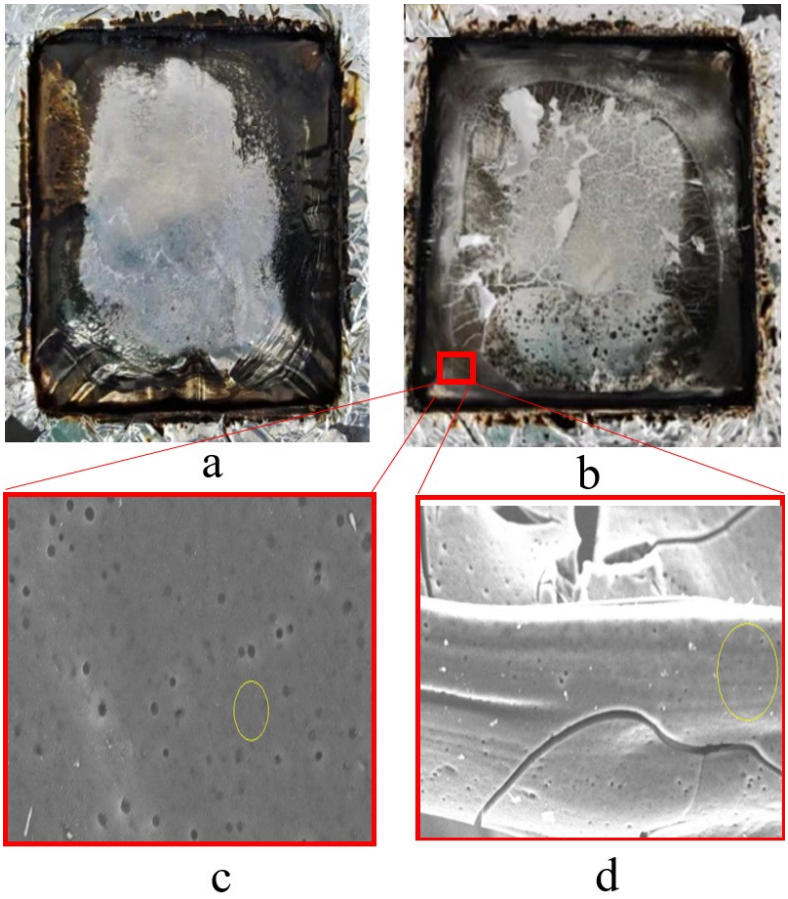

Fig. 7S. Digital images results of (a) pure PLA and (b) PLA/0.8% F-FR composites; SEM of the (c) inner and (d) outer surface of PLA/0.8% F-FR composites after cone-calorimeter tests

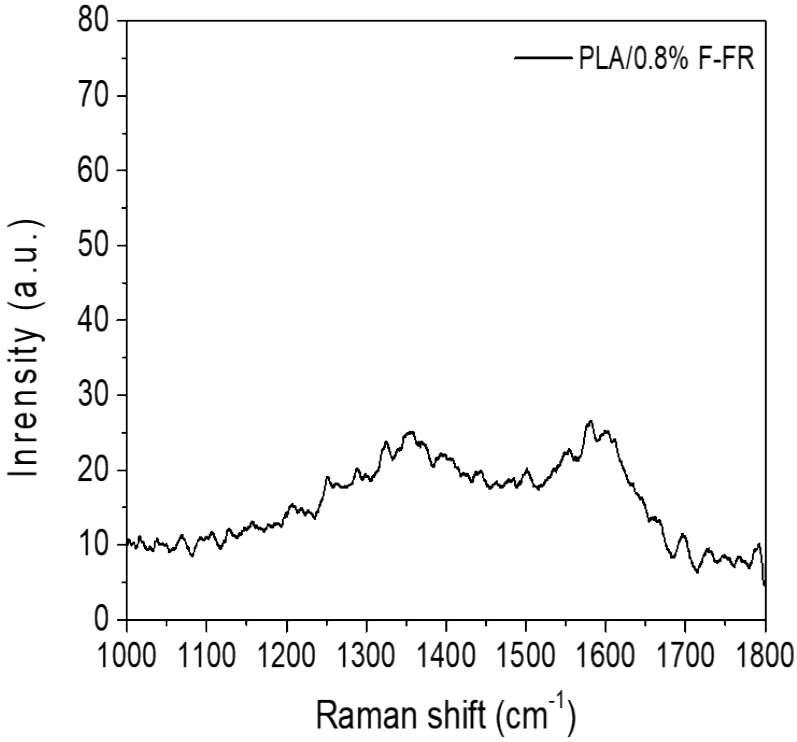

Fig. 8S. Raman result of PLA/0.8% F-FR composites after cone-calorimeter tests

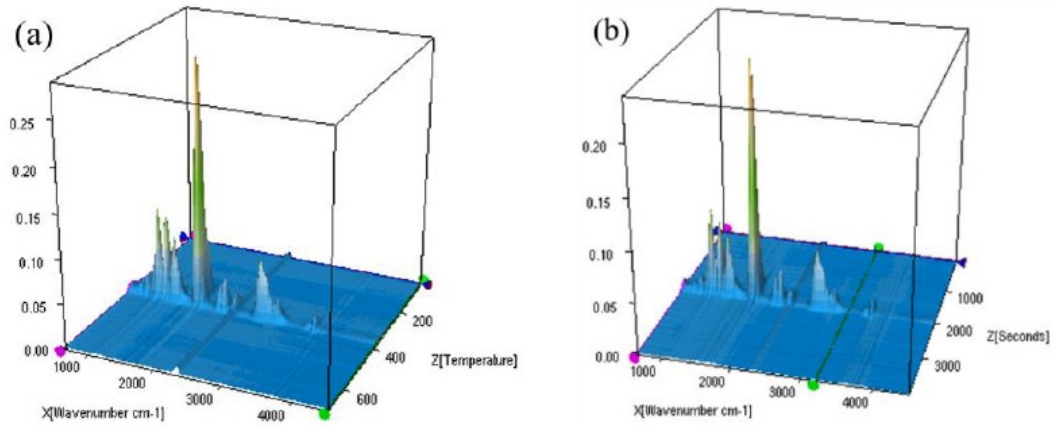

Fig. 9S. 3D image TG-FTIR of (a) pure PLA and (b) PLA/0.8% F-FR composites

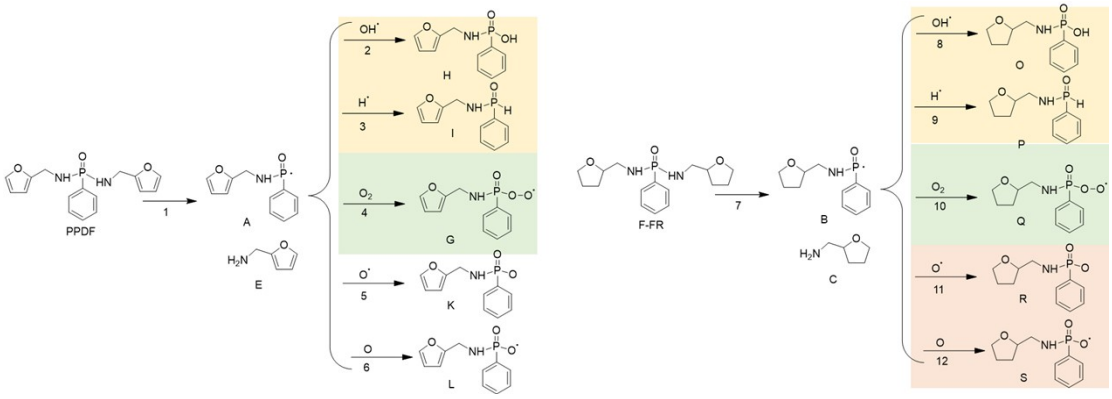

Fig. 10S. The possible pyrolysis of PPDF and F-FR

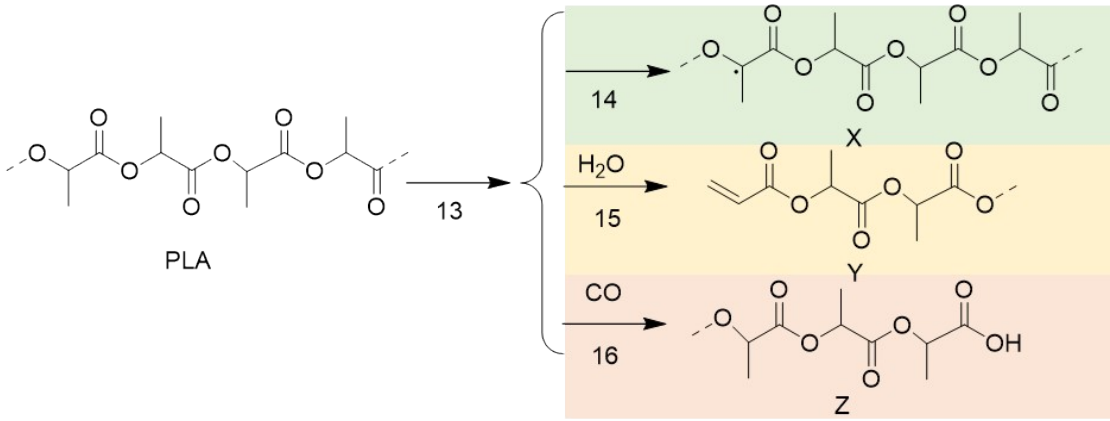

Fig. 11S. The possible pyrolysis of PLA

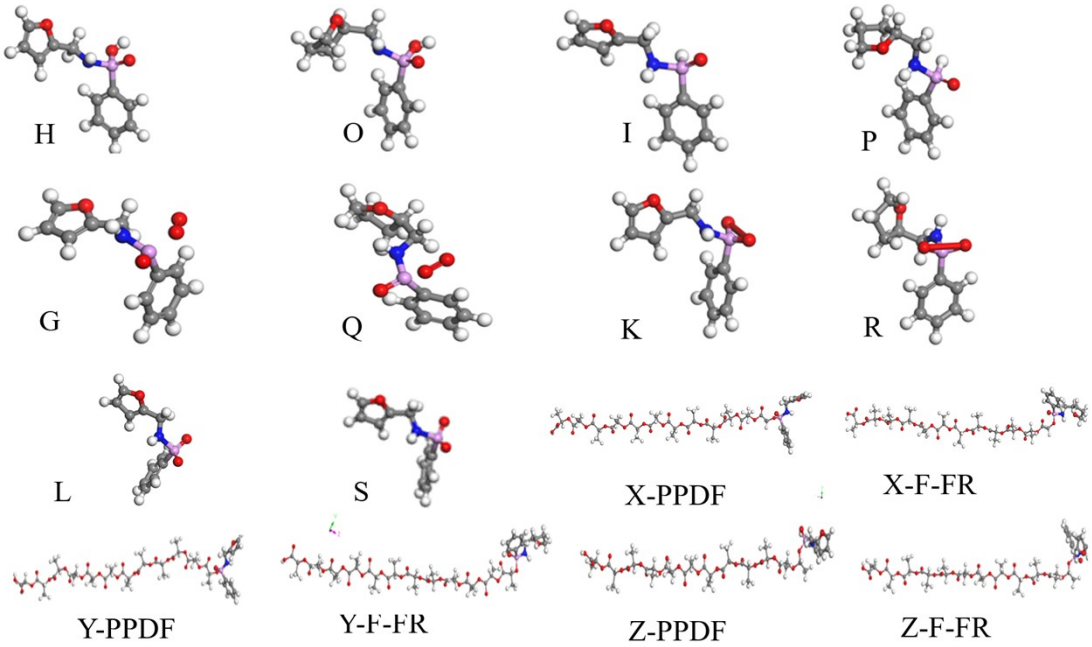

Fig. 12S. The degradation or pyrolysis products were simulated by Material Studio software

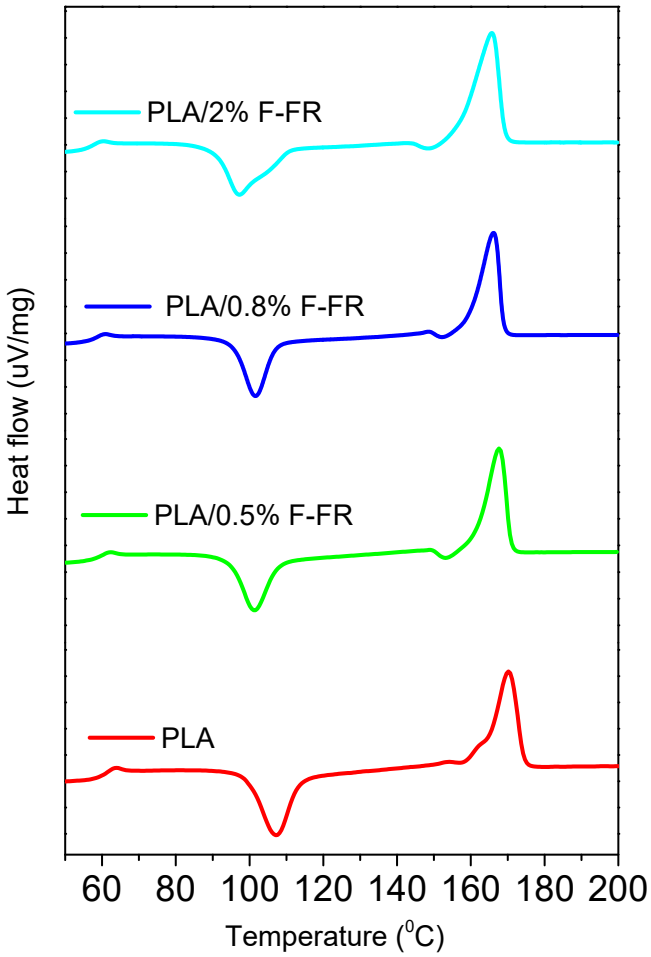

Fig. 13S. Non-isothermal crystallization results of pure PLA and PLA/F-FR composites

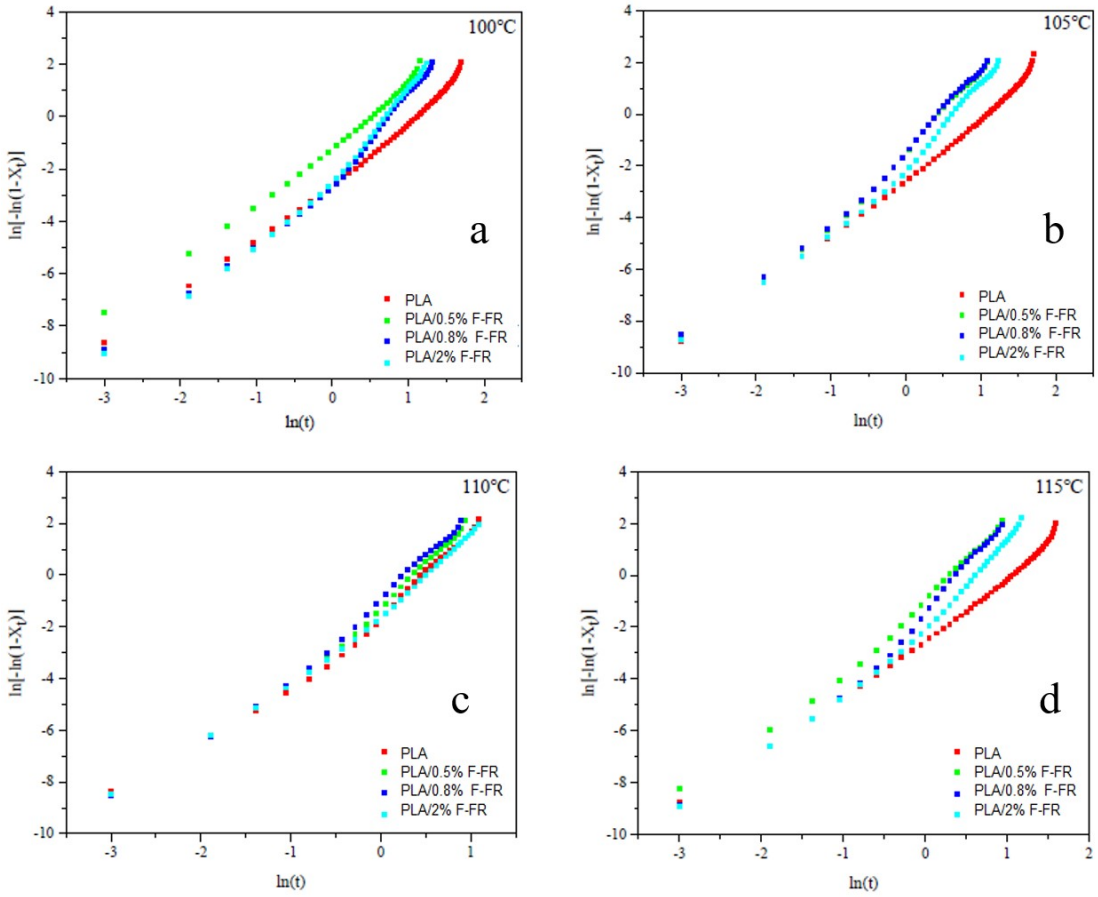

Fig. 14S. Isothermal crystallization of ln[-ln(1-Xt)] vs. ln(t) results of pure PLA and PLA/F-FR composites at (a)100℃, (b)105℃, (c) 110℃ and (d)115℃

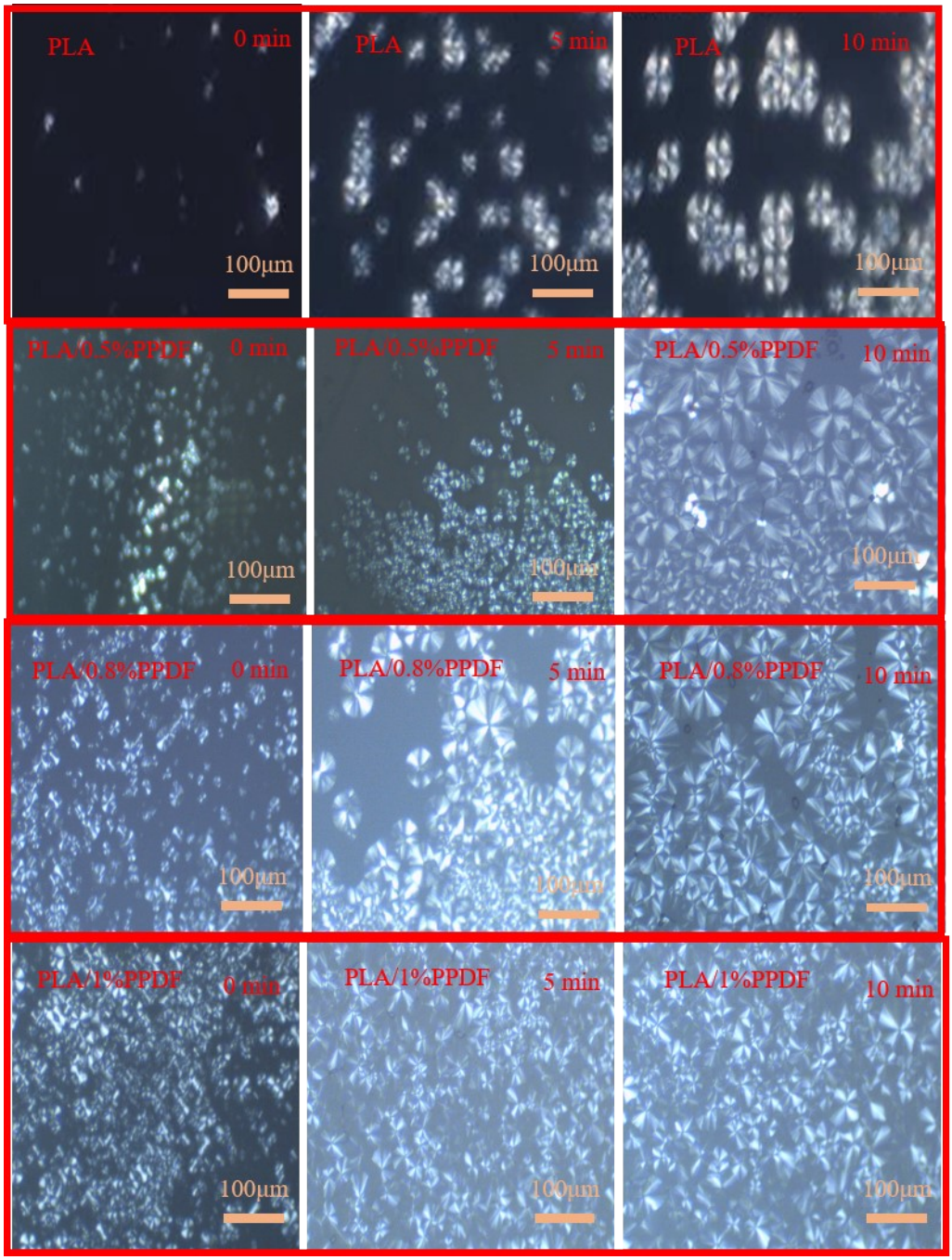

Fig. 15S. POM images of pure PLA and PLA/F-FR composites at 115 ˚C for 0, 5 and 10 min.

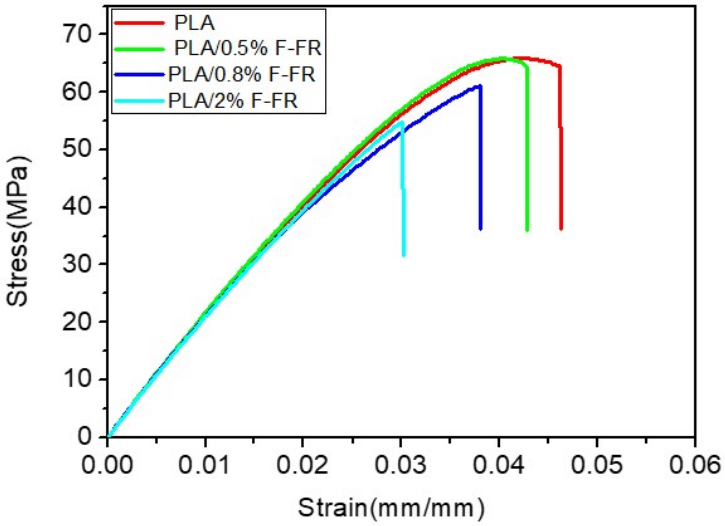

Fig. 16S The tensile results of PLA and PLA/F-FR composites

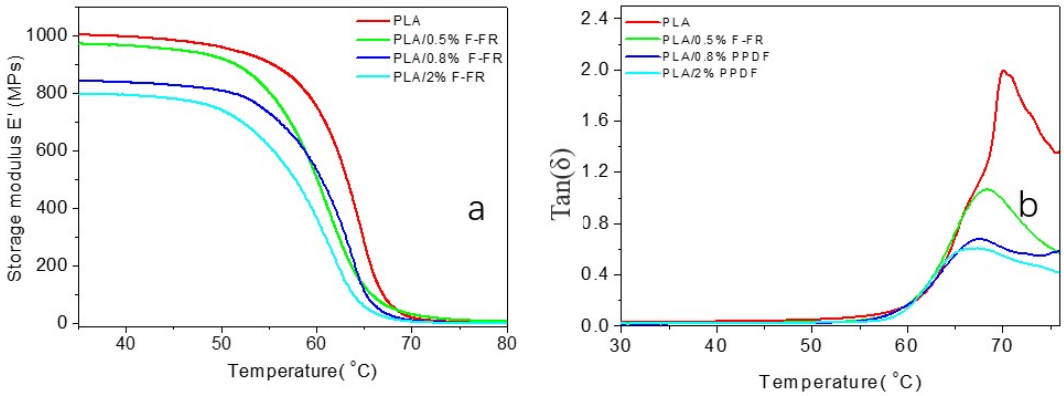

Fig. 17S The DMA results of PLA and PLA/F-FR composites

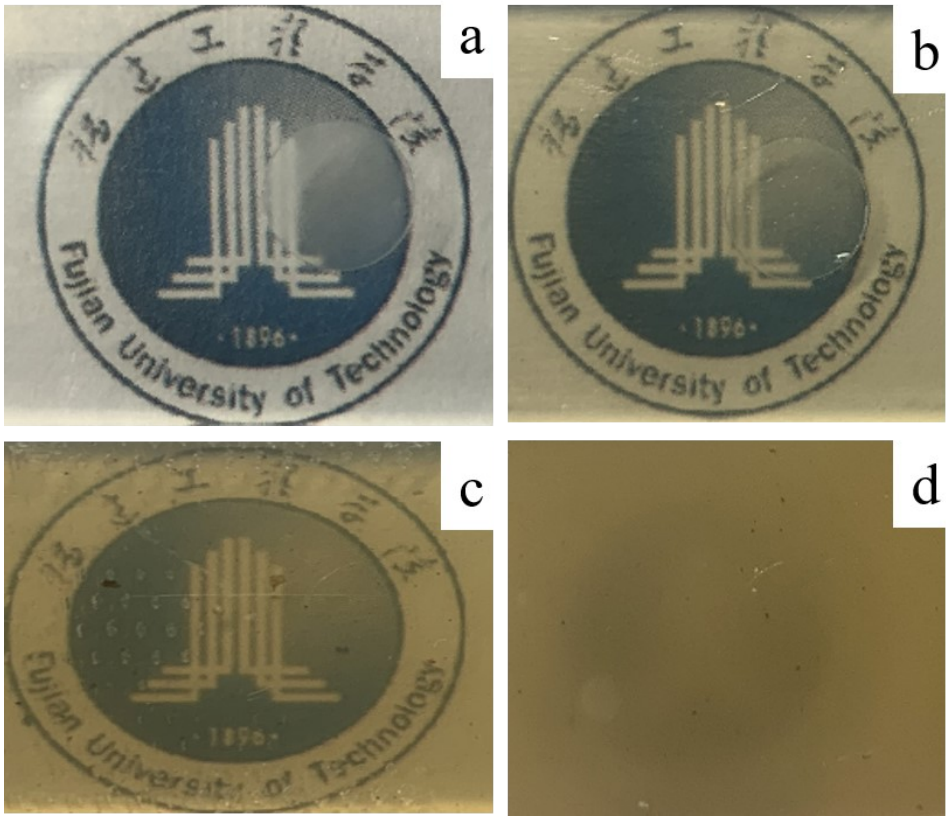

Fig. 18S. The transparency results of (a) pure PLA, (b) PLA/0.5%F-FR, (c) PLA/0.8%F-FR and (d)PLA/2%F-FR composites